ELSEVIER

Contents lists available at ScienceDirect

Combustion and Flame

journal homepage: www.elsevier.com/locate/combustflame



Competitive oxidation of methane and C₂ hydrocarbons discerned by isotopic labeling and laser absorption spectroscopy of CO isotopologues in shock-heated mixtures



Daniel I. Pineda a,b,1,*, Fabio A. Bendana R. Mitchell Spearrin

- a Department of Mechanical and Aerospace Engineering, University of California, Los Angeles (UCLA), Los Angeles, CA 90095, USA
- ^b Department of Mechanical Engineering, The University of Texas at San Antonio (UTSA), San Antonio, TX 78249, USA

ARTICLE INFO

Article history:
Received 4 September 2020
Revised 5 November 2020
Accepted 5 November 2020
Available online 17 November 2020

Keywords: Isotopic labeling Absorption spectroscopy Chemical kinetics Fuel chemistry

ABSTRACT

The competitive oxidation of methane with C₂ hydrocarbons of differing functional groups (alkane, alkene, and alkyne) was examined experimentally via combustion of isotopically-labeled fuel mixtures and laser absorption spectroscopy of carbon monoxide isotopologues. Quantitative species time-histories of the ¹²CO and ¹³CO isotopologues were measured simultaneously and in situ using laser absorption spectroscopy behind reflected shock waves, used for near-instantaneous heating and auto-ignition of binary mixtures containing equal carbon fractions of the different fuels. A driver extension and gas tailoring were employed on the shock tube facility to extend test times up to 30 milliseconds, enabling dilute ignition of the fuel blends over a range of temperatures from 1100-1800 K. Tested fuel mixtures were primarily fuel-rich to force the competition of carbon oxidation between the fuel components. The novel dataset of multi-isotopologue species time-histories were compared to available chemical mechanisms, revealing insights on the influence of each C2 fuel on methane ignition. The GRI-MECH 3.0 and Foundational Fuel Chemistry Model (FFCM-1) reaction models were modified to incorporate ¹³C reactions and species. Detailed comparison of the measurement data with FFCM-1 simulations revealed generally good agreement at elevated temperatures (>1500 K), with increasing divergence at lower temperatures, particularly for mixtures involving ethane and acetylene. Reaction pathway and sensitivity analysis of the variance between data and the modified mechanisms reveal key reactions likely responsible for the disagreements.

© 2020 The Combustion Institute. Published by Elsevier Inc. All rights reserved.

1. Introduction

Accurate and computationally-efficient chemical kinetic models are desired to design practical combustion systems operating with real fuels—usually blends of several different hydrocarbons—to meet performance and emissions targets in the transportation and power sectors [1]. In several advanced energy conversion devices—such as Homogeneous Charge Compression Ignition (HCCI) engines—ignition is governed by reaction kinetics and the overall reactivity of the fuel-air mixtures is much more sensitive to system thermochemistry (temperature, pressure, mixture composition) and fuel molecular structure than in traditional combustion systems [2,3]. This represents a significant challenge for modeling and system design, particularly at lower combustion temperatures

(<1500 K) where reaction kinetics can be more complex and are generally less well-understood. This study leverages a novel diagnostic method to examine kinetic behavior of select hydrocarbon mixtures, with a particular focus on discerning competitive oxidation at temperatures below 1200 K, relevant to real fuel combustion.

Modeling real fuels such as diesels or kerosenes remains a challenge in part due to the complex fuel compositions that may include hundreds of species of varying carbon number and functional group. Despite this heterogeneity, large hydrocarbons and mixtures thereof have been shown to decompose into a relatively smaller pool of similar fuel fragments [4–6]; the reactions of these fuel fragments are the rate-limiting steps in the combustion of higher hydrocarbons [7–9]. Although in principle this increases the tractability of the modeling problem, significant challenges remain in characterizing the combustion behavior of blends of even the smallest C_1 – C_2 hydrocarbons at lower temperatures, as significant coupling exists between the intermediates of different fuel components [10]. To examine this coupling, several investigators have

 $^{^{*}}$ Corresponding author at: Department of Mechanical Engineering, The University of Texas at San Antonio (UTSA), San Antonio, TX, 78249, USA.

E-mail address: daniel.pineda@utsa.edu (D.I. Pineda).

Experimental work performed during postdoctoral appointment at UCLA.

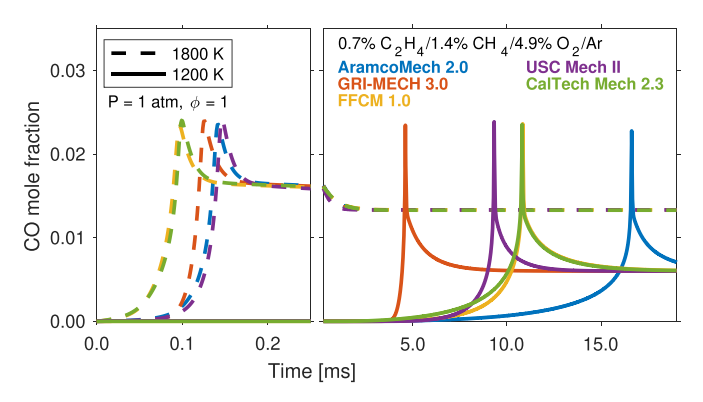


Fig. 1. Predictions of CO mole fraction evolution during constant-volume reaction of 0.7% C_2H_4 , 1.4% CH_4 , and 4.9% O_2 ($\phi\approx 1$) in Ar by various chemical kinetic mechanisms at 1 atm and 1800 K and 1200 K, plotted at different x axis scales on the left and right, respectively. Simulations performed using CANTERA 2.4.0 [50].

studied the effects of blending small C_1 – C_2 fuels together through a variety of experiments including but not limited to measurements of flame speeds [11–13], as well as of ignition delay times behind reflected shock waves [14–19]. Despite this experimental work and concurrent progress in chemical mechanisms, many reaction models which predict similar time-evolution of combustion species at high temperatures (>1800 K) yield significantly different predictions of time-to-ignition at lower temperatures (<1500 K), though peak CO mole fraction remains similarly predicted amongst the models. An example of this is shown in Fig. 1 for predictions of the time-evolution of CO, a key intermediate in the energy conversion process, during combustion of a methane-ethylene fuel blend.

Accurate prediction of CO formation and oxidation in combustion systems is critical for the development of practical energyconversion devices, owing to its importance in the determination of heat release and extinction behavior [8,20]. The predictive capability of reaction models for fuel oxidation can be evaluated through comparison with time-resolved species measurements behind reflected shock waves, often through optically-based measurement methods. Quantitative species time-histories can provide an additional granular constraint on kinetic models along with ignition delay times and flame speeds, which are aggregate measurements of overall combustion behavior [21]. Several experimental studies have reported measured species time-histories of CO during oxidation of hydrocarbons behind reflected shock waves, including many using laser absorption-based measurements [8,22-31], providing valuable experimental constraints and validation benchmarks with which to compare chemical reaction models. However, only a few of these studies considered fuel mixtures [26-28,31]; in many modern chemical reaction models available in the literature, significant uncertainties remain in several key elementary reactions involved in the production of CO at low temperatures, particularly reactions involving the formyl (HCO), vinyl (C_2H_3) , and ketenyl (HCCO) radicals [8,10,29,32–34]. These species are prominent in the oxidation of small C₁-C₂ fuel mixtures, including CH₄ and C₂H₄, as seen in the simplified reaction pathways shown in Fig. 2. These species participate in a much larger set of reactions and the relative contribution (i.e. branching fractions) of various fuel components in a mixture to the measured CO species time-histories becomes less clear when additional fuel components are added.

To address this ambiguity, the authors have developed a time-resolved laser absorption spectroscopy (LAS) measurement technique for simultaneous detection of multiple isotopologues to discern individual contributions of fuel components to the production of CO in the oxidation of multi-component fuel blends [35]. By isotopically-labeling specific component fuels of the overall fuel

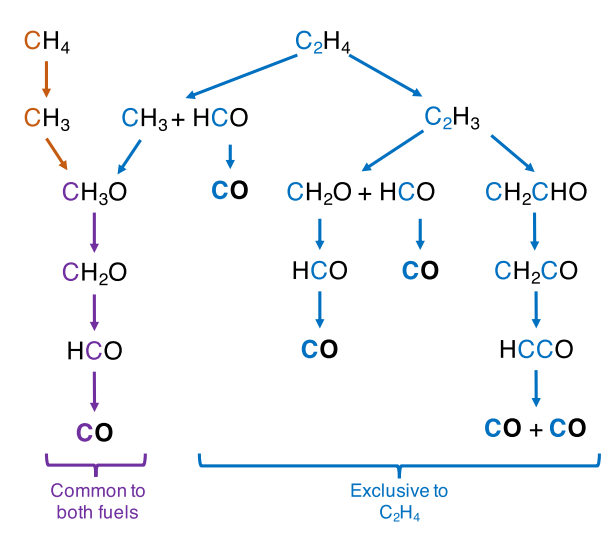


Fig. 2. Simplified reaction pathway for the oxidation of a CH_4/C_2H_4 blend into CO, with carbon atoms color-coded to correspond to source fuel molecule. CH_4 -exclusive pathways shown in orange, C_2H_4 -exclusive pathways shown in blue, and common pathways shown in purple. (For interpretation of the references to color in this figure legend, the reader is referred to the web version of this article.)

mixture and simultaneously measuring intermediates (both ¹²CO and ¹³CO), we can distinguish reaction pathways and respective rates by unambiguously identifying the parent fuels of intermediate species [36,37]. Figure 2 shows competing reaction pathways for the oxidation of CH_4 and C_2H_4 into CO-many more pathways to CO are observed for C2H4 than are observed for CH4, and the carbon atoms are color-coded to highlight the utility of the multi-isotopologue LAS technique in providing more information about specific reaction pathways. In previous work [35], we observed that ¹²CO (from ¹²C₂H₄) was produced both earlier than ¹³CO (from ¹³CH₄) and earlier than predicted by an isotopicallylabeled GRI-MECH 3.0 [38] reaction model in shock tube oxidation experiments performed at temperatures of 1500 K. In this work, we examine an expanded set of oxidizing fuel mixtures behind reflected shock waves at temperatures ranging from 1000-1800 K, incorporating mixtures that include additional C2 hydrocarbons: the alkane ethane (C_2H_6) and the alkyne acetylene (C_2H_2) . We primarily target the fuel-rich domain to force competitive oxidation among the component fuels, and for its relevance in fuel pyrolysis and soot formation.

The following sections of this paper describe the shock tube experimental setup and isotopic labeling and detection methods, followed by a presentation of the novel dataset capturing competitive oxidation of methane and C_2 hydrocarbons. The approach to modifying specific chemical mechanisms for isotopic labeling is also presented, and simulation results are compared to experimental data. A more detailed examination of the modified FFCM 1.0 mechanism is given for CH_4 - C_2H_4 blends, including reaction pathway and sensitivity analysis, while opportunities for mechanistic improvements are identified to capture kinetic behavior of blends with the other C_2 hydrocarbons.

2. Methods

This section describes the methods used to examine competitive oxidation of methane and different C_2H_X hydrocarbons behind reflected shock waves. We first detail the spectroscopic sensing methodology as well as the shock tube facility used for all experiments. Additionally, we describe the adaptation of chemical mechanisms for measurement comparison. Estimates of the

measurement uncertainty and model sensitivity are discussed in detail in Section 4.

2.1. Multi-isotopologue CO spectroscopy

Laser absorption spectroscopy (LAS) is a well-established optical diagnostic technique for shock tube kinetics studies, owing to its high time-resolution, species-specificity, and quantitative capability in the measurement of species and temperature. For a single quantum energy transition or line j, monochromatic light absorption through a uniform gas medium is governed by the Beer-Lambert law [39]:

$$\alpha_{\nu} = -\ln\left(\frac{I_t}{I_0}\right)_{\nu} = PS_j(T)X_{\text{abs}}L\varphi_{\nu} \tag{1}$$

where I_t/I_0 is the ratio of transmitted to incident light intensity at frequency ν [cm⁻¹], α_{ν} is the spectral absorbance at that frequency, P [atm] is the total pressure, $S_j(T)$ [cm⁻²/atm] is the temperature-dependent linestrength of transition j at temperature T [K], $X_{\rm abs}$ is the mole fraction of the absorbing species, L [cm] is the aggregate path-length of the absorbing medium, and φ_{ν} [cm] is the spectral lineshape of the transition.

The mole fractions of two isotopologues of carbon monoxide were measured here using a continuous wave (cw) distributed feedback quantum cascade laser (DFB-QCL, ALPES Lasers) targeting the P(0,31) and P(2,20) transitions of $^{12}C^{16}O$ and the P(0,22) and P(1,16) transitions of $^{13}C^{16}O$ near 4.9 µm [35]. A scanned-wavelength direct absorption technique was employed to rapidly scan over the spectral domain of interest, enabling integration in ν over each individual rovibrational transition. This yields a spectrally-integrated absorbance area A_j [cm $^{-1}$] for each transition j,

$$A_{j} = \int_{-\infty}^{+\infty} \alpha_{\nu} d\nu = PS_{j}(T) X_{abs} L$$
 (2)

eliminating dependence on lineshape φ_{ν} ($\int_{-\infty}^{+\infty} \varphi_{\nu} d\nu = 1$). Upon measuring multiple A_j for a given species, gas temperature can be determined through two-line thermometry, wherein the ratio of two A_j reduces to a ratio of $S_j(T)$, which is a function of T only [39]:

$$R = \frac{A_A}{A_B} = \frac{S_A(T)}{S_B(T)} = f(T) \tag{3}$$

Once T is known, Eq. (2) can be used to determine absorbing species mole fraction $X_{\rm abs}$, assuming independent knowledge of the pressure. Herein, temperature and mole fraction were measured spectroscopically once the signal-to-noise ratio (SNR) of the spectral transitions was high enough to perform the aforementioned two-line thermometry technique. Prior to this, temperature was obtained using shock relations and assuming isentropic compression of the measured pressure trace. As demonstrated in prior work [35], good agreement in the initial post-shock conditions is achieved with the two methods. Both temperature values are reported in the proceeding data.

The optical setup for the present work is shown in Fig. 3. The laser light pitch and catch system, including the QCL, photodetector (Vigo PVI-4TE-5), optical bandpass filter (Spectrogon, 4960±148 nm), and lens is the same as in prior work targeting these CO isotopologues [35], with a notable exception: To increase the modulation depth of the QCL at high scan rates (and subsequently the robustness in baseline fitting), we employ a diplexed RF modulation technique developed by our group using bias-tee circuitry [40]. In this work, we injection-current modulate the QCL with a sine wave at 50 kHz, resulting in an effective temperature and species measurement rate of 100 kHz when performing spectral fitting on both the upscan and downscan. Represen-

tative detector signal waveforms illustrating this modulation during a shock tube oxidation experiment are shown in the top right of Fig. 3. Employing the bias-tee circuitry at a 50 kHz scan rate results in a modulation depth of approximately 1.2 cm $^{-1}$, capturing the $^{12}\mathrm{C}^{16}\mathrm{O}$ and $^{13}\mathrm{C}^{16}\mathrm{O}$ transitions of interest. A representative plot of experimentally-measured spectral absorbance for a single laser scan period is shown in Fig. 4 for the upscan. A corresponding spectral fit using the Voigt lineshape model for the targeted transitions is also shown, yielding low residuals (< 2%) for all experiments performed for this study. Lastly, all measurement uncertainties shown in this study are computed using the approach outlined in the appendix of our previous work [35].

2.2. Shock tube experiments

Here we use a shock tube facility to serve as a near constantvolume reactor to observe chemical kinetics with minimal influence of fluid dynamics. Because of the Arrhenius behavior of many chemical reactions in combustion, examining lower-temperature (1100-1200 K) ignition behavior and kinetic rates requires significantly longer test times compared to high-temperature combustion (>1800 K). Additionally, variations in either temperature or pressure during a test can significantly affect the observed kinetics. As an example, a temperature increase as small as 1% at 1500 K can lead to a 25% error in the measured rate coefficient for the dissociation of NO2 [41]. Consequently, conducting low-temperature chemical kinetics experiments requires both extended test times (> 5 ms) and well-controlled and characterized thermodynamic conditions. In a conventional shock tube, the reflected shock wave creates a near-instantaneous and spatiallyhomogenous high-temperature reactor with precisely known thermodynamic conditions (typically $< \pm 1\%$ in pressure and temperature) [42]; however, the usable test time is often limited to 1-3 ms [21] due to physical dimensional constraints that lead to wave interactions or non-ideal gas dynamics such as boundary layer growth [43]. To extend test times, such that low-temperature combustion kinetics are observable, conventional shock tubes may require physical modification of the geometry and/or gas mixture optimization to mitigate effects that terminate constant pressure test times. A notable distinction in the present shock tube study from our prior work [35] is the implementation of a 19.76 ft. driver extension, variable-area driver inserts, and tailored driver gases; the judicious combination of which enable significantly longer duration test times (up to 30 ms) than are achievable in the shock tube's standard configuration [44].

The high-enthalpy shock tube used in this study is shown in Fig. 3 and is also described in previous work by the authors [35,45,46]. The facility consists of a high-pressure driver section and a low-pressure driven (test gas) section, which are separated by either a polycarbonate or metal diaphragm. When the diaphragm ruptures due to pressure-induced strain, an incident shock wave forms and propagates into the driven sectioncompressing and heating the test gas and imposing a bulk velocity in the direction of the moving shock. Additionally, an expansion wave travels into the driver and the contact surface between the driver and driven gases propagates into the driven section (although at a much lower velocity). When the incident shock wave reaches the end wall of the driven section, it reflects back towards the driver, stagnating the flow and compressing and heating the test gas even further. This creates near-constant temperature and pressure conditions and initiates the test time for the kinetics experiments conducted in this work.

The pressure time history at the measurement location (near the end wall) determines the test time and can be used to assess uniformity of the thermodynamic conditions during a test. The test time typically ends when either the expansion fan reflects

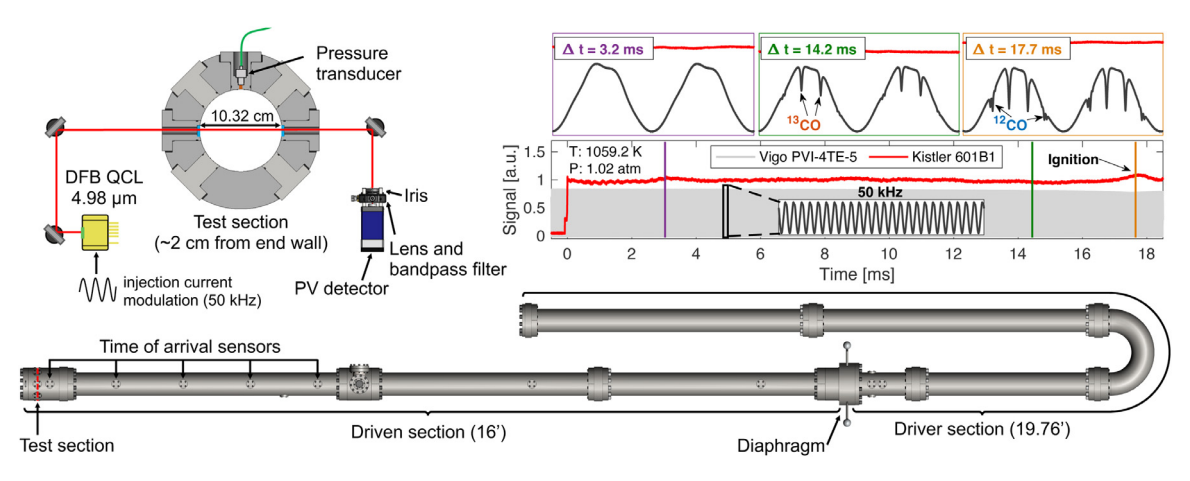


Fig. 3. Shock tube facility with driver extension used for extended test times. A cross-section of the test section with optical setup is shown alongside representative test data. Example pressure and detector data highlight the diagnostic techniques ability to discern competitive oxidation, via ¹²CO and ¹³CO measurements, in a reacting mixture of 1.14% ¹³C₂H₄, 1.14% ¹²C₂H₆, 5.71% O₂, and 18.4% He in argon.

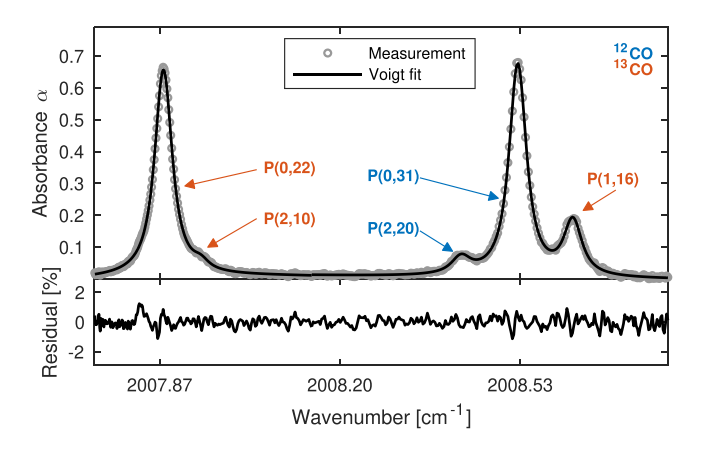


Fig. 4. Example scanned-wavelength Voigt fitting of data in a shock tube oxidation experiment.

off the driver end wall and returns to the driven section-changing the thermodynamic conditions at the measurement location-or the contact surface and reflected shock wave interact, sending another shock or expansion wave back towards the measurement test section. To delay the reflected expansion fan arrival and extend the total test time, a 19.76 ft. driver extension, shown in Fig. 3, was used for all the measurements conducted in this study. The use of the driver extension enables reflected shock test times up to 30 ms, ideal for studying low-temperature combustion chemistry. Additionally, more uniform thermodynamic conditions were achieved by using a tailored driver gas mixture (75%He/N2) to mitigate contact surface-reflected shock wave interactions along with variablearea driver inserts to minimize the pressure rise, dP/dt, (and the associated temperature rise [47]) caused by factors such as boundary layer growth and shock attenuation. Driver gas tailoring can minimize expansion or compression at the test section when the reflected shock wave interacts with the contact surface. This is achieved by blending a lower speed-of-sound gas, such as N2, with He, such that the pressures across the contact surface following the passage of the reflected shock wave, are identical. To minimize dP/dt, variable-area driver inserts were designed [48] to partially reflect expansion waves back to the test section where the chemical kinetic studies are being conducted. The pressure decrease from the expansion waves helps offset the pressure rise caused by nonidealities in the test section. Combined, these modifications result in an approximate factor of 10 increase in the achievable test times compared to our standard shock tube configuration and are particularly useful for studying low-temperature combustion chemistry, where reaction rates are relatively slow. The results can be directly observed in Fig. 3, where ignition at 1059.2 K and 1.02 atm occurs on the order of 18 ms, with pre-ignition chemistry observed as early as 8 ms.

To conduct experiments, the driver and driven sections of the shock tube are connected to rotary vane roughing pumps (Alcatel Adixen 2021i) and a turbomolecular pump (Varian V550) to reach ultimate pressures $< 1 \times 10^{-4}$ torr and remove trace amounts of any contaminating species. The driven and driver sections are then filled with the test gas mixture and tailored gas, respectively. The tailored driver gas contained 75% He balanced in N2 and was supplied by Airgas. Test gas mixtures were barometrically prepared with capacitance manometers (Baratron 627D) with an uncertainty of 0.12% of reading in an agitated mixing tank. All test gas mixtures were prepared in an Ar or 18.4% He/Ar bath gas and targeted a nearly equal number of carbon atoms corresponding to each carbon isotope $(67\%CH_4/33\%C_2H_X)$, where X = 2, 4, 6. $^{12}CH_4$, $^{12}C_2H_2$, ¹²C₂H₄, ¹²C₂H₆, O₂, He, and Ar gases were supplied by Airgas with purities of 99.97%, 99.6%, 99.9995%, 99.99%, 99.994%, 99.997%, and 99.99%, respectively. ¹³CH₄ and ¹³C₂H₄ gases were supplied by Sigma-Aldrich with purities of 99% and 99%. Competitive oxidation experiments were conducted over a range of temperatures (1000-1800 K) at near-atmospheric pressures (0.5-1.5 atm). Combustion kinetics were compared and analyzed based off the thermometry and species measurements discussed in Section 2.1. Additionally, ¹²CO and ¹³CO production rates assisted in evaluating the validity and sensitivity of several chemical kinetic models (GRI-MECH 3.0 [38] and FFCM-1 [49]) for the different fuels and conditions considered herein.

2.3. Chemical kinetic modeling

For model comparison and evaluation, we modified both the GRI-MECH 3.0 [38] mechanism and the Foundational Fuel Chemistry Model (FFCM-1) [49] to account for isotopic labeling of carbon atoms. In GRI-MECH 3.0, this increased the number of species from 53 to 117 and the number of reactions from 325 to 886. For FFCM-1, the number of species increased from 38 to 85 and the number of reactions increased from 291 to 926. We initially examine these somewhat reduced models as they possess a small enough number of reactions and species so as to be tractable for isotopic labeling, and we provide the isotopically labeled FFCM-1 model (in the CANTERA CTI format) in the supplementary material.

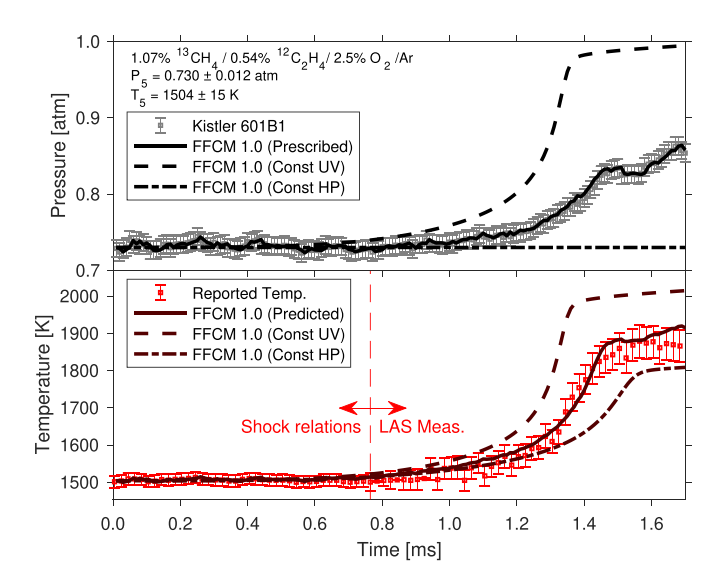


Fig. 5. Pressure (top) and temperature (bottom) prescribed / predicted by models and measured in experiments in a shock tube oxidation experiment. 0.54% C_2H_4 , 1.07% CH_4 , and 2.5% O_2 ($\phi \approx 1.5$) in argon.

These mechanisms include the various fuel components of interest, but it should be noted that the models were primarily developed for predicting methane combustion and have had little to no validation against C_2 fuel blends. Additional larger mechanisms are also employed for comparison of the global kinetic timescales (i.e. ignition delay times).

In addition to the chemical model, the simulation technique for a shock tube experiment can affect the quality of comparison with measurements. Measurements of ignition experiments behind reflected shock waves are often compared with zero-dimensional reactor models, assuming a constant internal energy / volume (constant U, V) or a constant enthalpy / pressure (constant H, P) thermochemical process. These models are only valid in reflected shock wave experiments for reacting mixtures with minimal heat release, and so these experiments are typically highly diluted in inert gas, such as argon. It is often desirable to increase the concentration of reactants in these experiments, either to enable the mixture to ignite within the test time allowed by the shock tube, or to increase absorbance for a more robust species measurement. To enable model comparison with experiments utilizing higher concentrations of reactants, we employ a split-timestep reactor model in Cantera [50] similar to that developed for Chemkin by Li et al [51]. At the beginning of each time step, the zero-dimensional mixture is at an initial temperature T, pressure P, and composition X. During the first part of each timestep, the mixture is allowed to react while holding volume V and internal energy U constant, resulting in new values of temperature T', pressure P', and composition X'. Following this constant volume reaction, the mixture is isentropically expanded (or compressed) assuming a frozen mixture composition X' from the model-predicted pressure P' to the experimentally measured pressure P_{meas} :

$$V_{final} = V' \left(\frac{P_{meas}}{P'}\right)^{1/\gamma} \tag{4}$$

This is performed using Cantera's wall() function, and has the effect of isentropically increasing or decreasing the mixture temperature to a value T_{final} , which is used as initial temperature T for the next timestep. A representative assessment of the split-timestep reactor model's performance is shown in Fig. 5 for a reactive $\mathrm{CH_4/C_2H_4/O_2/Ar}$ mixture at approximately 1500 K and 0.73 atm. The modified split-timestep reactor model displays an enhanced accuracy relative to both the constant-volume and

constant-pressure reactor models in predicting the temperature evolution of the system.

For the split-timestep reactor model currently implemented in Cantera 2.4.0, a small computational performance impact is observed for reactor simulations without sensitivity analyses, but this impact is magnified significantly for reactor simulations utilizing sensitivity analyses. Sensitivity analyses of the FFCM-1 reaction model were conducted using multiple reactor simulations. For each experiment, a full sensitivity analysis considering all 926 reactions for a constant volume reactor model was first conducted to determine time-resolved normalized sensitivity coefficients for each 12 CO and 13 CO concentration with respect to reaction rate constants k_i :

$$S_{k,CO} = \frac{k_i}{CO} \cdot \frac{\partial CO}{\partial k_i}$$
 (5)

This constant UV reactor model is initiated with the experimentally-determined reflected shock conditions T_5 and P_5 , as well as the molar composition X. The Foundational Fuel Chemistry Model effort provides uncertainty factors for each reaction, f_k [49]. We can utilize these f_k values to weight our normalized sensitivity coefficients, so as to specifically highlight reactions that deserve more attention when comparing model predictions with experimental measurements:

$$S_{k,CO}^f = f_k \cdot S_{k,CO} \tag{6}$$

We rank the reactions by their uncertainty-weighted sensitivity, and consider the top 50 in a subsequent sensitivity analysis utilizing the split-timestep reactor model discussed previously. We use these sensitivity analyses to identify key reactions which can be isolated by the multi-isotopologue LAS method.

3. Results

3.1. Competitive oxidation of methane with ethylene

The oxidation of methane (CH₄) and ethylene (C₂H₄) mixtures were investigated behind reflected shock waves at multiple temperatures for both fuel-rich ($\phi=1.5$) and stoichiometric ($\phi=1.0$) equivalence ratios. The experiments are performed at reflected shock temperatures between 1100 and 1800 K and pressures between 0.5 and 1.5 atm. In most cases, included those shown here, the initial mole fractions of each fuel component were adjusted to give an equal number of carbon atoms, such that at longer time scales approaching equilibrium, the mole fractions of carbon monoxide are expected to equalize according to simulations. This provided a quantitative check on the magnitudes of each measured isotopologue. The convergence of the measurements at longer times can be readily observed in the figures throughout this section.

Temperature and species time-histories of ¹²CO and ¹³CO during shock tube oxidation experiments for fuel-rich ($\phi = 1.5$) mixtures of ¹³CH₄ and ¹²C₂H₄ are shown in Fig. 6 for a series of postshock temperatures. As initial temperature progressively decreases, the oxidation process slows overall and timescales of the component fuels increase in separation. At 1726 \pm 19 K, $^{13}\text{CH}_4$ and $^{12}\text{C}_2\text{H}_4$ are experimentally observed to oxidize into ¹³CO and ¹²CO at very similar rates. At 1504 ± 15 K, the reaction timescales are separated, with ¹²C₂H₄ oxidizing into ¹²CO earlier than ¹³CH₄ and at a faster rate. At 1210 ± 11 K, the reaction timescale separation widens further, such that the concentration of ¹²CO reaches a value greater than seven times that of ¹³CO at half the ignition delay time. At the lower two initial temperatures of 1504 ± 15 K and 1210 ± 11 K, there is an eventual convergence in magnitude and rate of ¹²CO and ^{13}CO production at ≈ 1.3 ms and ≈ 7.9 ms, respectively, indicating a transition from lower-temperature oxidation to rapid

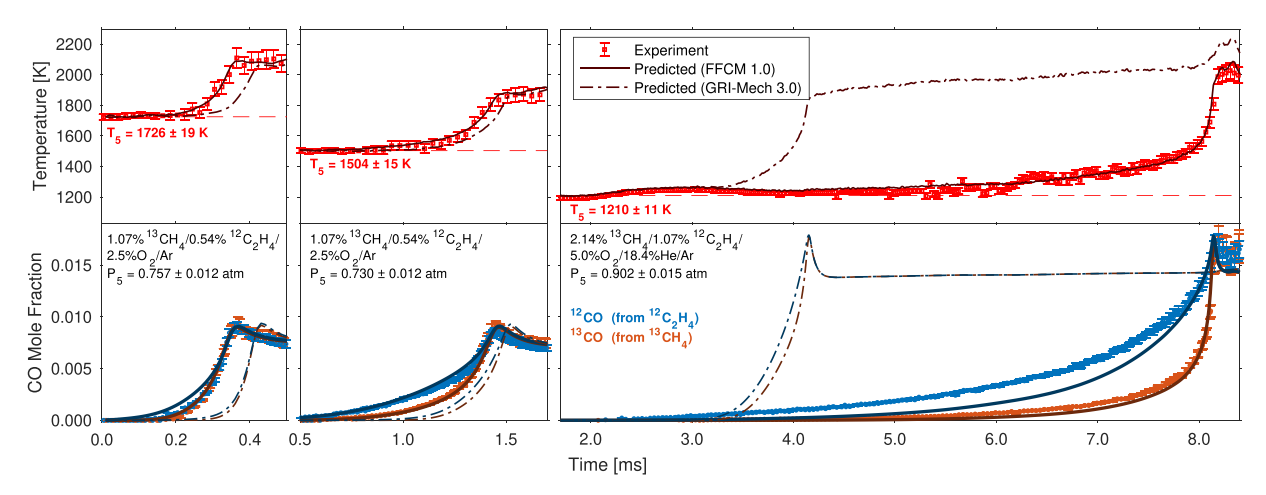


Fig. 6. Measurements and predictions of temperature (top) and CO mole fraction evolution (bottom) during oxidation behind reflected shock waves of $C_2H_4/CH_4/O_2$ reactive mixtures ($\phi \approx 1.5$) in Ar and Ar/He bath gases. t=0 denotes passage of reflected shock. Some data points are omitted for reader clarity, and reflected shock temperatures decrease from left to right. The data are plotted at different x axis scales to better examine temperature and CO evolution.

ignition behavior. In all cases, rapid rise in concentration of the CO isotopologues is accompanied by a corresponding rise in temperature. Overall, the results support established understanding that ethylene possesses an increased ability to consume oxygen relative to methane at lower temperatures, increasing mixture reactivity and reducing ignition delay in fuel mixtures [11,13,18].

The measurement data is overlaid with CO isotopologue simulations from both the modified FFCM-1 and GRI-MECH 3.0 models. We first note that measured peak values of CO match very well with both mechanisms. The increasing separation in reaction timescale is predicted by both reaction models, though the FFCM-1 model more accurately predicts the extent of the increasing separation than the GRI-MECH 3.0 model. The ignition delay time is also much better predicted by FFCM-1. To better compare the time-resolved model predictions with measured species time-histories prior to ignition, we slightly time-shift experimental profiles (via adjustment of initial temperature/pressure within experimental uncertainty) such that the measured peak mole fractions of CO correspond to the numerical peak mole fractions predicted by FFCM-1 [29,35]. FFCM-1 slightly overpredicts the early ^{12}CO production at 1726 ± 19 K and 1504 ± 15 K despite accurately predicting the production of ¹³CO within experimental uncertainty. By contrast, FFCM-1 underpredicts the oxidation rate of ^{12}CO from $^{12}\text{C}_2\text{H}_4$ at 1210 ± 11 K, despite qualitatively capturing the fuel-specific behavior of low- and high-temperature oxidation. In general, the isotopically-labeled FFCM-1 chemical kinetic model outperforms the isotopically-labeled GRI-MECH 3.0 model at all temperatures examined, particularly at lower temperatures. This is unsurprising, as the GRI-MECH effort largely did not target temperatures much below 1200 K [38] and was not validated against C₂H₄. For this reason, as well as the availability of uncertainty factors for each reaction in FFCM-1 (facilitating subsequent sensitivity analysis), we restrict our detailed modeling comparisons to FFCM-1 in the rest of this work.

The competitive oxidation behavior of the different fuel components persists in the increased availability of oxygen. Figure 7 compares the results of two shock tube oxidation experiments at similar temperatures of \approx 1160 K but with different equivalence ratios. During oxidation of stoichiometric mixtures of $^{12}C_2H_4$ and $^{13}CH_4,\ ^{12}CO$ appears earlier than $^{13}CO,$ just as in the fuel-rich mixtures, demonstrating that the reaction pathways of oxidation are not unique to fuel-rich competitive oxidation conditions. As with the fuel-rich condition, the FFCM-1 reaction model accurately predicts the formation of $^{13}CO,$ while slightly under-predicting ^{12}CO in the earlier stages of ignition. The reduction in absolute magni-

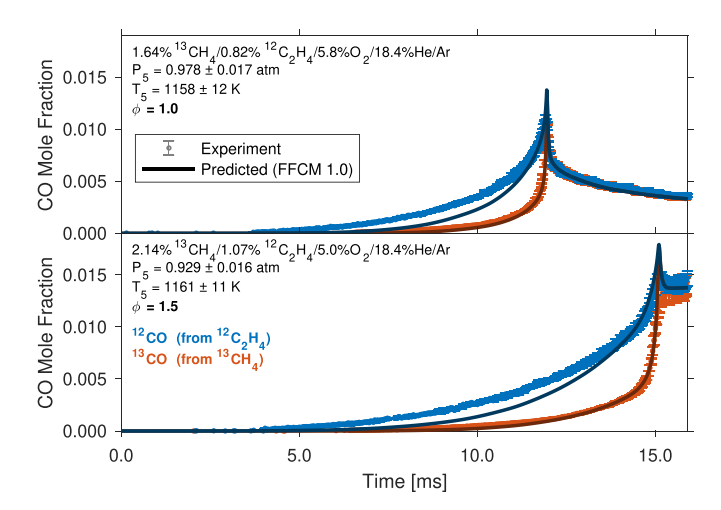


Fig. 7. Measurements and predictions of CO mole fraction evolution during oxidation behind reflected shock waves of both stoichiometric ($\phi = 1.0$, top) and fuelrich ($\phi = 1.5$, bottom) $C_2H_4/CH_4/O_2$ reactive mixtures in an Ar/He bath gas. t = 0 denotes passage of reflected shock. Some data points are omitted for reader clarity.

tude of CO concentration for both isotopologues is well predicted by the model at both equivalence ratios.

Overall the FFCM-1 model predictions are in relatively good agreement with the results, and the temporal evolution of 12 CO is largely captured despite underprediction of early CO formation at lower temperatures. It should be noted that FFCM-1 was not optimized with C_2H_4 as a target [8,49], and has explicitly not been recommended for use beyond H_2 , H_2 /CO, H_2 O, and H_4 combustion [49]. However, the reaction model remarkably appears to capture the kinetic behavior of the H_4 /C₂H₄ mixtures quite well, especially for the predicted time to peak CO concentration.

3.2. Competitive oxidation of CH₄ with different C₂ fuels

To examine the effect of functional group on the competitive oxidation behavior of CH_4/C_2H_X fuel mixtures, mixtures of CH_4 with the alkane C_2H_6 , the alkene C_2H_4 , and the alkyne C_2H_2 were prepared, maintaining a constant ratio of carbon-to-oxygen across the different fuel combinations. Time-histories of both CO isotopologues for two shock tube oxidation experiments of near-stoichiometric mixtures of $^{13}CH_4/^{12}C_2H_4$ ($\phi=1.00$) and $^{13}CH_4/^{12}C_2H_6$ ($\phi=1.07$) are shown in Fig. 8 for similar temper-

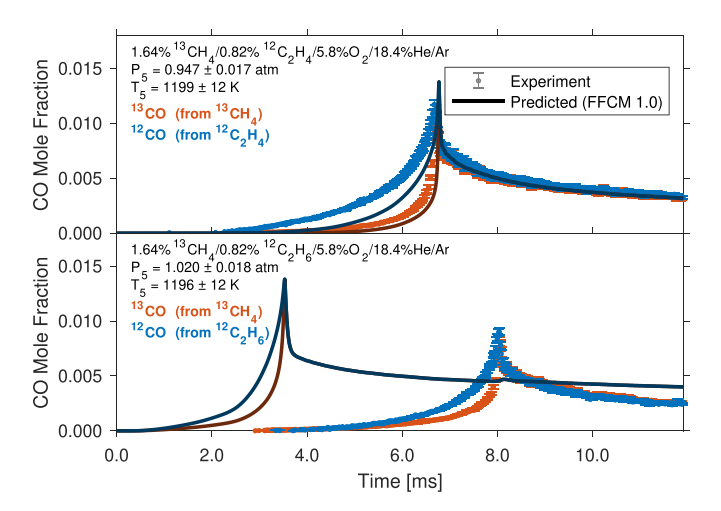


Fig. 8. Measurements and predictions of CO mole fraction evolution during oxidation behind reflected shock waves of near-stoichiometric reactive mixtures of $C_2H_4/CH_4/O_2$ (top) and $C_2H_6/CH_4/O_2$ (bottom) in an Ar/He bath gas. t=0 denotes passage of reflected shock. Some data points are omitted for reader clarity.

atures of \approx 1200 K. Note that although the equivalence ratios are different, the carbon/oxygen ratios, O2 concentration, and dilution of reactants for the two tests are the same. The ${}^{13}\text{CH}_4/{}^{12}\text{C}_2\text{H}_6$ mixture is observed to ignite slightly later than the ¹³CH₄/¹²C₂H₄ mixture despite higher pressures, highlighting the greater reactivity of C₂H₄ under near-stoichiometric conditions. While both C2H6 and C2H4 promote earlier oxidation of CH4 at lower temperatures than would be observed on its own, the effect of each C_2H_X fuel is distinctly different. In the $^{13}CH_4/^{12}C_2H_6$ mixture, ^{13}CO initially appears at very similar concentrations as ¹²CO, indicating that both fuels are oxidizing to CO at similar rates in the earlier stages of combustion. After about 5 ms, however, the concentration of ¹²CO outpaces that of ¹³CO, although not to the same extent that is observed for the ¹³CH₄/¹²C₂H₄ mixture. The FFCM-1 reaction model significantly overpredicts the oxidation rate of the CH₄/C₂H₆ alkane fuel blend, beyond which is explained by experimental uncertainty-overprediction of peak CO concentration by state-of-the-art reaction models at the stoichiometric condition was also noted by Mathieu et al. in their investigation of CH₄ oxidation [29]. Notably, the difference of ignition delays between the two mixtures examined here is less pronounced than that predicted by the model.

In fuel-rich conditions, competition for available O_2 is greater, magnifying the distinct behavior of each C2HX fuel on the overall evolution of both CO isotopologues. Time-histories of temperature and both CO isotopologues for three shock tube oxidation experiments of fuel-rich mixtures of $^{13}\text{CH}_4/^{12}\text{C}_2\text{H}_4$ ($\phi = 1.50$), $^{13}\text{CH}_4/^{12}\text{C}_2\text{H}_6~(\phi=1.60)$, and $^{13}\text{CH}_4/^{12}\text{C}_2\text{H}_2~(\phi=1.40)$ are shown in Fig. 9 for similar temperatures of \approx 1150 K. As with the nearstoichiometric experiments shown in Fig. 8, the carbon/oxygen ratio, O₂ concentration, and reactant dilution are the same among the three tests shown. Unlike in the near-stoichiometric experiments, however, the ${}^{13}\text{CH}_4/{}^{12}\text{C}_2\text{H}_6$ mixture is observed to ignite slightly earlier than the ${}^{13}\text{CH}_4/{}^{12}\text{C}_2\text{H}_4$ mixture. Additionally, the $^{13}\text{CH}_4/^{12}\text{C}_2\text{H}_6$ mixture is observed to ignite at a similar time as the ${}^{13}\text{CH}_4/{}^{12}\text{C}_2\text{H}_2$ mixture, although uncertainties in initial temperature preclude a definite conclusion. The ¹³CH₄/¹²C₂H₂ mixture displays the earliest temperature rise and earliest ¹²CO formation, indicating more pre-ignition heat release than the other mixtures at these temperatures. The largest separation in oxidation timescales between the two CO isotopologues is observed for the $^{13}\text{CH}_4/^{12}\text{C}_2\text{H}_4$ mixture, followed by the $^{13}\text{CH}_4/^{12}\text{C}_2\text{H}_2$ and the ¹³CH₄/¹²C₂H₆ mixture. As was observed in the near-stoichiometric

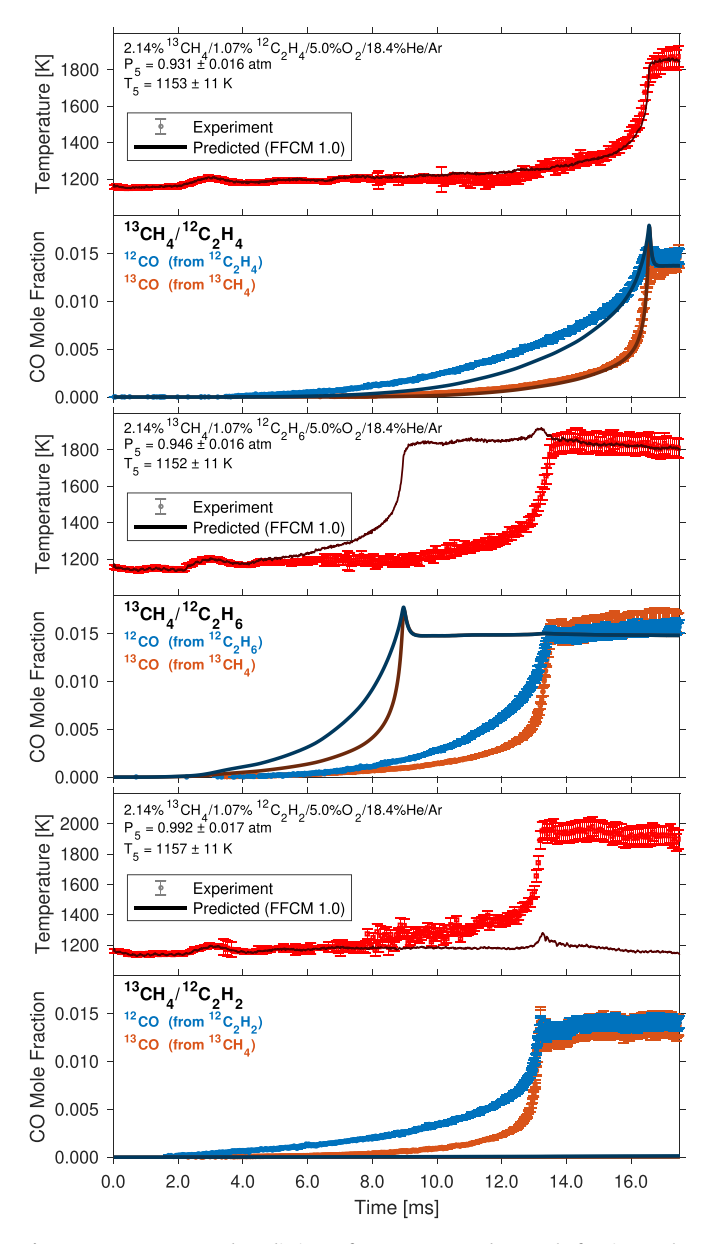


Fig. 9. Measurements and predictions of temperature and CO mole fraction evolution during oxidation behind reflected shock waves of fuel-rich reactive mixtures of $C_2H_4/CH_4/O_2$ (top), $C_2H_6/CH_4/O_2$ (middle), and $C_2H_2/CH_4/O_2$ (bottom) in an Ar/He bath gas. t=0 denotes passage of reflected shock. Some data points are omitted for reader clarity.

cases for the alkane mixture containing $^{12}C_2H_6$, ^{13}CO initially appears at very similar concentrations as ^{12}CO , indicating that the reactions involved in $^{12}C_2H_6$ oxidation also serve to promote the oxidation of $^{13}CH_4$. Additionally, the FFCM-1 significantly overpredicts the oxidation rate of the alkane mixture while underpredicting the oxidation rate of the $^{13}CH_4/^{12}C_2H_2$ mixture. As C_2H_2 was not a target fuel and only a limited set of C_2H_6 was included in the FFCM-1 optimization effort [49], the disagreement is not unexpected.

To check whether or not isotopic effects may be occurring on the timescales associated with the measurements presented in this study, a mixture of $^{13}\text{C}_2\text{H}_4$ and $^{12}\text{CH}_4$ —analogous to the fuel-rich ($\phi=1.5$) mixture shown previously in Figs. 6, 7, and 9—was prepared to compare species evolution behind reflected shock waves. The results of a representative shock tube oxidation experiment at \approx 1160 K are shown in Fig. 10. The results show evolution of both

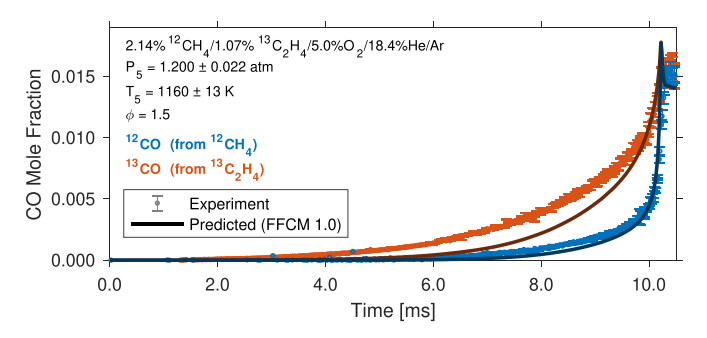


Fig. 10. Measurements and predictions of CO mole fraction evolution during oxidation behind reflected shock waves of a fuel-rich ($\phi=1.5$) $^{13}\text{C}_2\text{H}_4/^{12}\text{CH}_4/\text{O}_2$ reactive mixture in an Ar/He bath gas. t=0 denotes passage of reflected shock. Some data points are omitted for reader clarity.

CO isotopologues that is reversed from the previous tests: 13 CO now appears earlier and in higher concentrations than 12 CO, suggesting that the 13 C₂H₄ is oxidizing earlier and more rapidly than 12 CH₄, and—most importantly—that this behavior prior to ignition is unaffected by any observable isotopic effects. Additionally, the isotopically-labeled FFCM-1 reaction model generally captures the relative oxidation of the two CO isotopologues. The time to ignition is observed to be shorter than the analogous experiment in Fig. 9; this is attributed to a difference in initial pressure in the experiments.

The results shown in this section highlight representative data from each mixture. A total of 40 shock tube tests were run over a range of conditions and trends are examined more holistically in the following section.

4. Discussion

Here we examine global kinetic scales (ignition delay times) and more granular reaction pathways via the time-resolved multi-isotopologue species measurements. A focused sensitivity analysis is performed on the $\text{CH}_4/\text{C}_2\text{H}_4$ mixtures, and some future research directions are suggested.

4.1. Ignition delay times

To take advantage of the availability of larger detailed mechanisms (for which isotopic labeling is outside the scope of this investigation), we examine measured global kinetic timescales and compare several modern detailed chemical reaction models against experimental data for binary fuel mixtures, several of whichparticularly those of CH₄/C₂H₄-have not previously been reported for these temperatures, pressures, mixture and equivalence ratios, even without isotopic labeling. Besides FFCM-1 [49], these models include USC Mech II [52], AramcoMech 2.0 [53], and Caltech Mech 2.3 [54]. For these comparisons, the time-resolved summation of both CO isotopologue mole fractions is assumed to behave the same as an unlabeled mixture. We compare an ignition delay time, $\tau_{i\sigma n}$, defined here as the time between the passage of the reflected shock and the time of peak CO concentration. This readily quantifiable metric facilitates comparison between model predictions and experimental observations in this work.

To examine the different models' predictive capability relative to one another for the temperature range of interest, constant volume reactor ignition simulations were performed for several examined mixtures assuming an initial pressure—averaged across all experiments for a given test gas composition as $P_{\text{avg,mix}}$ —isentropically compressed using an averaged dP/dt pressure rise (1.5%/ms). This scaling of the initial pressure and temperature accounts for the pre-ignition pressure rise associated with the

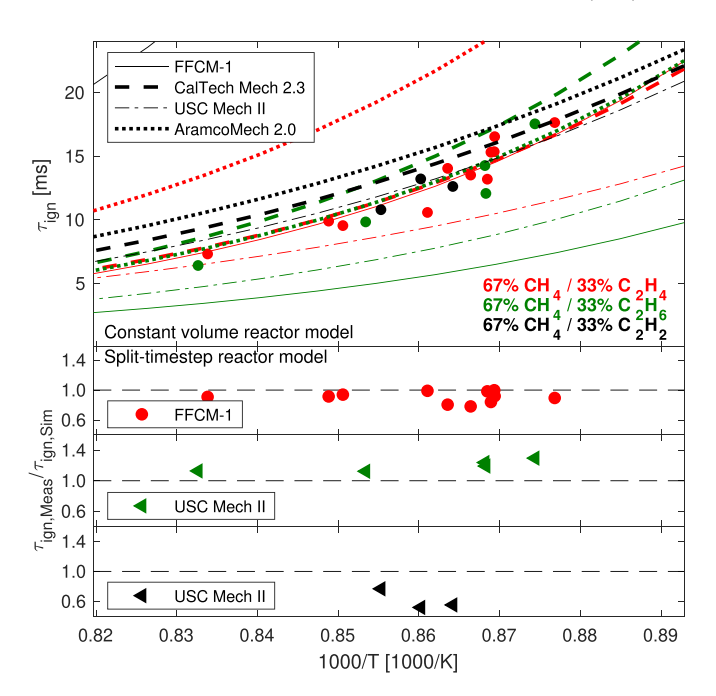


Fig. 11. Temperature dependence of predicted and experimentally observed global kinetic timescales for different mixtures of CH_4/C_2H_X hydrocarbons assuming constant volume ignition (top) alongside relative predictive capability of various reaction models when using the split-timestep reactor model described in Section 2.3 (bottom).

energetic mixtures examined in this study while reducing the influence of test-specific pressure behavior, allowing for easier comparison amongst model predictions. Constant-volume reactor $\tau_{\rm ign}$ predictions for different $^{13}{\rm CH_4}/^{12}{\rm C_2H_X}/{\rm O_2}/{\rm Ar}/{\rm He}$ mixtures at constant carbon-to-oxygen ratio (C/O = 0.856) are shown in the top of Fig. 11 alongside measured $\tau_{\rm ign}$. In the top plot of Fig. 11, the experimentally-determined $\tau_{\rm ign,Meas}$ is simply scaled by ($P_{\rm 5,Meas}/P_{\rm avg,mix}$) to facilitate test-to-test comparison across a range of pressures:

$$\tau_{\rm ign} = \left(\frac{P_{\rm 5,Meas}}{P_{\rm avg,mix}}\right) \tau_{\rm ign,Meas} \tag{7}$$

Note that this is a relatively small correction as most tests were near atmospheric pressure (1 atm), and at these elevated temperatures, $\tau_{\rm ign} \propto 1/P$. Beyond this, we do not attempt to determine any scaling laws for the experimental data. As mentioned previously, the carbon/oxygen ratio, O_2 concentration, and reactant dilution are the same across tests, with the goal to examine variations associated with fuel structure.

Somewhat surprisingly, in the experimental global kinetic timescale data shown in Fig. 11, there are no obvious fuel-specific effects, suggesting that-at least for the binary mixtures, temperatures, and pressures examined in this study—the structure of C₂H_X hydrocarbons does not strongly affect overall τ_{ign} . This contrasts with several reaction models that predict a much greater influence of fuel components on the ignition delay than is experimentally observed. FFCM-1 predicts shorter ignition delay times for mixtures containing C_2H_6 than for those containing C_2H_4 , which are predicted to ignite much more quickly than mixtures containing C_2H_2 . USC Mech-II predicts the same fuel-ordering in τ_{ign} , though the fuel-specific influence is reduced. Similarly, AramcoMech 2.0 predicts that mixtures containing C2H6 ignite faster than the others, although it predicts that those containing C2H4 react most slowly. Of the models examined, the Caltech Mech 2.3 reaction model predicts the most similar au_{ign} behavior among the binary fuel mixtures, and the predictions for the CH₄/C₂H₄ mixture are

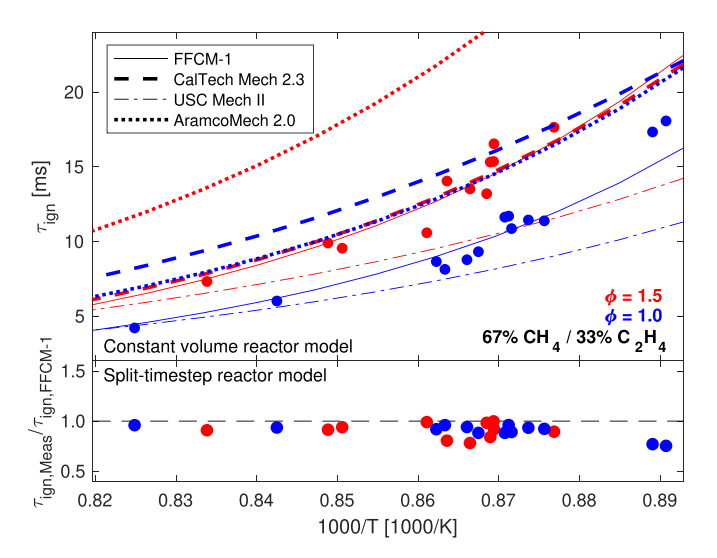


Fig. 12. Temperature dependence of predicted and experimentally observed global kinetic timescales for binary CH_4/C_2H_4 mixtures at two different equivalence ratios assuming constant volume ignition (top) alongside relative predictive capability of various reaction models when using the split-timestep reactor model described in Section 2.3 (bottom).

nearly identical to those of FFCM-1 for the temperature range examined.

For an assessment of the ability of the models to predict CO time history and ignition delay while considering shock tube nonidealities such as pressure variation, we use the split-timestep reactor model developed in Section 2.3 to determine $\tau_{ign,Sim}$ predicted by each chemical model. Relative predictive capability of the most accurate models with respect to $\tau_{ign,Meas}$ are shown in the bottom of Fig. 11 for all CH₄/C₂H_X mixtures as a ratio of observed versus predicted values. In this analysis, the data are not time-shifted to compare time-resolved speciation of CO. Of the reaction models, FFCM-1 is observed to best capture both the quantitative and qualitative temperature-dependent ignition behavior of the fuel-rich ¹³CH₄/¹²C₂H₄ fuel mixtures, which was shown in Section 3. Despite the overprediction relative to FFCM-1 shown for the constant-volume simulations of ¹³CH₄/¹²C₂H₆ mixtures, USC Mech-II is observed to best capture their behavior when considering experimental pressure variation, although the disagreement increases at lower temperatures. When considering time-varying pressure in the shock tube experiments, nearly all of the models significantly underpredict the reactivity of the ¹³CH₄/¹²C₂H₂ fuel mixtures for the tests shown, exhibiting a delayed formation of CO relative to experimental observations, similar to what was observed in Fig. 9. Of the models, USC Mech-II is observed to have the best relative predictive capability, as shown in the bottom plot of Fig. 11. Overall, the best model for acetylene mixture underpredicts reactivity, the best model for ethane overpredicts reactivity, while for ethylene mixtures the best model (FFCM-1) very closely predicts the ignition delay.

To gain more insight with respect to competitive oxidation, we can further examine a single binary fuel combination, $^{13}\text{CH}_4/^{12}\text{C}_2\text{H}_4$. Constant-volume reactor $\tau_{\rm ign}$ predictions for $^{13}\text{CH}_4/^{12}\text{C}_2\text{H}_4/\text{O}_2/\text{Ar}/\text{He}$ mixtures at two different equivalence ratios ($\phi=1.0,1.5$) are shown in the top of Fig. 12 alongside measured $\tau_{\rm ign}$. A distinct separation in reaction timescales is observed between the fuel-rich and stoichiometric mixtures of the fuel blends, with the stoichiometric mixtures igniting earlier than the fuel-rich mixtures. As expected, there is an increase in ignition delay as temperatures decrease, accompanied by a divergence in $\tau_{\rm ign}$ predicted by the models. Most of the models, with the exception of Caltech Mech 2.3, predict faster ignition for the sto-

ichiometric equivalence ratio. For the fuel-rich mixtures, Caltech Mech 2.3 and FFCM-1 predict similar ignition behavior with respect to temperature-dependence, while the other models either underpredict (USC Mech-II) or overpredict (AramcoMech 2.0) ignition delay at lower temperatures. Relative predictive capability of FFCM-1 with respect to $au_{ign,Meas}$ is shown in the bottom of Fig. 12 for both fuel-rich and stoichiometic mixtures as a ratio of observed versus predicted values. As was shown in Section 3, the FFCM-1 reaction model generally demonstrates excellent agreement with experimental observations for binary CH₄/C₂H₄ mixtures, with many tests exhibiting agreement of ignition delay time within 5%. It should be noted that the increase in measurement scatter in the top of Fig. 12 relates to variation of initial test pressure and variation throughout the test time. When incorporating the split-timestep model, as shown in the residual plot, scatter is reduced and trends are more clear. While the FFCM-1 model performs quite well, there is a somewhat increasing overprediction of the ignition delay time with decreasing temperature that is outside of measurement scatter, though additional measurements at lower temperatures are needed to confirm this trend.

4.2. $CH_4-C_2H_4$ oxidation pathway analysis

The generally good agreement in ignition delay between the predictions of the split-timestep reactor model using FFCM-1 and the measured CO time-histories for binary fuel mixtures of CH₄/C₂H₄ enables a more granular sensitivity analysis of CO production, examining the different isotopologues to identify reactions responsible for disagreement during early oxidation. As CO is near the end of the overall oxidation process, many reactions common to the oxidation of all fuels-including those with large uncertainty factors f_k —are expected to be revealed as sensitive to its production; however, the ability to track each carbon isotope independently enables isolation of reactions which can be prioritized for further optimization. For example, experiments for which ¹³CO mole fraction agrees with numerical predictions, while ¹²CO mole fraction is lower than numerical predictions, prompt investigation into specific reactions for which increasing rates would produce relatively more ¹²CO than ¹³CO. To identify these reactions, we calculate the uncertainty-weighted sensitivity coefficients for the difference between ¹²CO and ¹³CO:

$$S_{k,\Delta CO}^{f} = \frac{f_k \cdot k_i}{{}^{12}CO - {}^{13}CO} \cdot \frac{\partial \left({}^{12}CO - {}^{13}CO\right)}{\partial k_i}$$
 (8)

This can be expressed in terms of the sensitivity coefficients defined previously in Eqs. (5) and (6):

$$S_{k,\Delta CO}^{f} = \frac{{}^{12}\text{CO} \cdot S_{k,{}^{12}\text{CO}}^{f} - {}^{13}\text{CO} \cdot S_{k,{}^{13}\text{CO}}^{f}}{{}^{12}\text{CO} - {}^{13}\text{CO}}$$
(9)

Time-resolved uncertainty-weighted isotopologue-difference sensitivity coefficients of selected reactions in the FFCM-1 chemical model for high temperature oxidation—spanning almost the entire duration of the experiment shown in the left of Fig. 6—are shown in Fig. 13. In the high-temperature experiment, the concentration of 12 CO just prior to ignition was slightly overpredicted by the model. Reactions with relatively uncertain rate constants that are candidates for adjustment include a few containing the formyl (HCO) and vinylidene (12 CC) radicals:

$$H_2^{12}C^{12}C + O_2 \longleftrightarrow 2H^{12}CO$$
 (R185)

$$^{12}C_2H_2 + M \longleftrightarrow H_2^{12}C^{12}C + M$$
 (R176)

$$^{12}C_2H_4 + M \longleftrightarrow H_2 + H_2^{12}C^{12}C + M$$
 (R237)

For reader convenience, we label the selected reactions in the text according to their reaction number in the original unlabeled

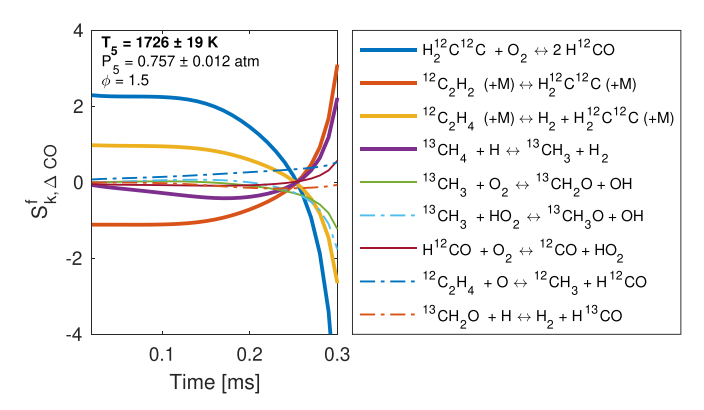


Fig. 13. Time-resolved $S_{k,\Delta CO}^f$ for selected reactions in an oxidation experiment at 1726 K. Dash/line styles simply help distinguish the respective reactions.

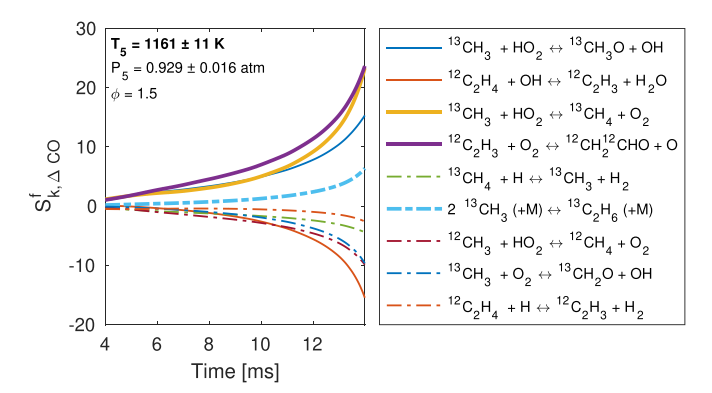


Fig. 14. Time-resolved $S_{k,\Delta CO}^f$ for selected reactions in an oxidation experiment at 1161 K. Dash/line styles simply help distinguish the respective reactions.

FFCM-1 reaction model. At the peak CO concentration, the denominator in Eq. (9) drops to zero as the predicted concentrations of ^{12}CO and ^{13}CO become nearly equal, and the sensitivity analysis provided by $S_{k,\Delta\text{CO}}^f$ becomes less informative. After the peak CO concentration, the uncertainty-weighted isotopologue-difference sensitivity coefficients of the reactions for both CO are very similar, and so and neither isotopologue is significantly more sensitive than the other to any of the reaction rates, and $S_{k,\Delta\text{CO}}^f$ drops to zero, though this is not shown in Fig. 13.

At lower temperatures, different reactions become much more significant. Figure 14 shows the uncertainty-weighted isotopologue-difference sensitivity coefficients of selected reactions for low temperature oxidation, corresponding to the experiment shown in the top of Fig. 7. In this plot, we highlight the region of the experiment near 10 ms, since that is where the greatest model disagreement is observed. In this experiment, the concentration of ¹²CO prior to ignition was largely underpredicted by FFCM-1, while the concentration of ¹³CO was predicted to within experimental uncertainty, allowing for identification of the the following reactions:

$$^{12}C_2H_4 + OH \longleftrightarrow ^{12}C_2H_3 + H_2O$$
 (R243)

$$^{12}C_2H_3 + O_2 \longleftrightarrow ^{12}CH_2^{12}CHO + O$$
 (R205)

$$^{12}\text{CH}_3 + \text{HO}_2 \longleftrightarrow ^{12}\text{CH}_4 + \text{O}_2$$
 (R104)

$$^{12}C_2H_4 + H \longleftrightarrow ^{12}C_2H_3 + H_2$$
 (R239)

Some key reactions involving the vinyl (C_2H_3) radical are observed. Notably, $S^f_{k,CO}$ for reaction R205 is large for both ^{12}CO and ^{13}CO (at

10 ms, 6.619 and 4.794, respectively). A reaction pathway analysis of the FFCM-1 chemical model near the same point in the ignition process (10 ms) shows that most (>60%) of the ^{12}C from $^{12}C_2H_4$ follows a path through the vinyl (C_2H_3) radical. Most of this is by reaction R243 with OH ($\approx\!72\%$), followed by reaction R239 with H ($\approx\!20\%$), and both of these reactions have been identified in the sensitivity analysis. Once C_2H_4 becomes C_2H_3 , about 24% of this C_2H_3 reacts with O_2 to form CH2CHO in reaction R205. Reaction R205 is one of several of C_2H_3 with O_2 ; these have been investigated by Goldsmith et al. [32], who determined that uncertainties in barrier heights on the $C_2H_3O_2$ potential energy surface result in a significant uncertainty in the temperature at which reaction R205 dominates all other competing reaction pathways.

While increasing the relatively uncertain rate of reaction R205 would increase ¹²CO more than ¹³CO, doing so without consideration of other sensitive reactions would cause ¹³CO to be overpredicted by the model. Other prominent reactions in Fig. 14 include low temperature pathways for ¹³CH₄ oxidation:

$$^{13}\text{CH}_3 + \text{HO}_2 \longleftrightarrow ^{13}\text{CH}_4 + \text{O}_2$$
 (R104)

$$2^{13}CH_3 + M \longleftrightarrow {}^{13}C_2H_6 + M$$
 (R112)

Adjusting these rates could increase the difference between ¹²CO and ¹³CO concentration (currently underpredicted in the experiment); however, this would do so by decreasing ¹³CO concentration rather than increasing ¹²CO concentration. Since ¹³CO concentration is well-predicted by the model, other rates should be prioritized in model optimization.

Notably, reactions containing ¹³C are often observed to have high sensitivity coefficients with respect to ¹²CO production, and vice-versa—this is often because these reactions consume or produce other species, such as the radicals OH, O, H, or HO₂, which are highly influential to the oxidation of all fuels. In this way, the multi-isotopologue technique provides increased granularity in the sensitivity analysis.

5. Conclusions

The competitive oxidation kinetics of methane (CH₄) with C₂ hydrocarbons of differing functional groups (alkane, alkene, and alkyne) was investigated via time-resolved measurements of carbon monoxide isotopologues (12CO and 13CO) in shock-heated isotopically-labeled fuel mixtures. Fuel-rich mixtures of methane with acteylene (C_2H_2) , ethylene (C_2H_4) , and ethane (C_2H_6) were examined by isotopically labeling one of the fuels with ¹³C. Shock tube auto-ignition experiments were conducted over a range of temperatures from 1100-1800 K and near-atmospheric pressures (0.5-1.5 atm). In aggregate this has yielded a novel dataset with more granular constraints than prior efforts (including, to the authors' knowledge, the first species time history measurements for these binary mixtures) that may be used as validation targets in mechanism refinement. In particular, recent studies in the HyChem effort [7–9] have shown that large fuel pyrolysis produces large amounts of methane and ethylene, further promoting the relevance of the reported measurements. In order to compare chemical models to measurement data, two mechanisms for small hydrocarbons fuels (GRI-MECH and FFCM-1) were modified in this work to include isotopically-labeled reactions and species. A modified mechanism—available in the supplementary material for FFCM1 may be used to identify reactions for future investigation, including those which may exhibit isotope effects. Other larger mechanisms were also employed to evaluate the global kinetics (ignition delay). When holding carbon/oxygen ratio and dilution constant, it was found that the different fuel-rich binary mixtures exhibited very similar ignition delay times, contrasting the stronger divergence

predicted by the models. A similar convergence has been observed for larger real fuel blends of highly variable composition [55].

The Foundational Fuel Chemistry Model was found to be in very good agreement for ignition delay of the $\mathrm{CH_4/C_2H_4}$ fuel mixtures at both stoichiometric and fuel-rich conditions, extending the validation range of the mechanism; however, the modified mechanism consistently under-predicted initial CO formation from ethylene oxidation at lower temperatures. A rigorous sensitivity analysis was performed to identify key reactions that may be responsible for the disagreement weighted by their uncertainty in the mechanism. While this work stops short of adjusting the rate constants, a framework is presented for future work towards mechanism refinement using the isotopic labeling approach, and additional validation data—complete with measurement uncertainties—are included as supplementary material.

Declaration of Competing Interest

The authors declare that they have no known competing financial interests or personal relationships that could have appeared to influence the work reported in this paper.

Acknowledgments

All experiments detailed in this work were performed at the Laser Spectroscopy and Gas Dynamics Laboratory at the University of California, Los Angeles, and are supported by the Doctoral New Investigator program of the American Chemical Society Petroleum Research Fund (59315-DNI6), as well as by the U.S. National Science Foundation, Award No. 1752516. DIP was supported in part by NSF AGEP Award No. 1306683. The authors acknowledge the assistance of Kevin K. Schwarm and Christopher C. Jelloian during the shock tube experiments.

Supplementary material

Supplementary material associated with this article can be found, in the online version, at doi:10.1016/j.combustflame.2020.11. 006.

References

- [1] S.M. Sarathy, A. Farooq, G.T. Kalghatgi, Recent progress in gasoline surrogate fuels, Prog. Energy Combust. Sci. 65 (2018) 67–108, doi:10.1016/j.pecs.2017.09.
- [2] F.L. Dryer, Chemical kinetic and combustion characteristics of transportation fuels, Proc. Combust. Inst. 35 (1) (2015) 117–144, doi:10.1016/j.proci.2014.09. 008
- [3] M.D. Boot, M. Tian, E.J. Hensen, S. Mani Sarathy, Impact of fuel molecular structure on auto-ignition behavior design rules for future high performance gasolines, Prog. Energy Combust. Sci. 60 (2017) 1–25, doi:10.1016/j.pecs.2016. 12.001.
- [4] E. Ranzi, M. Dente, A. Goldaniga, G. Bozzano, T. Faravelli, Lumping procedures in detailed kinetic modeling of gasification, pyrolysis, partial oxidation and combustion of hydrocarbon mixtures, Prog. Energy Combust. Sci. 27 (1) (2001) 99–139, doi:10.1016/S0360-1285(00)00013-7.
- [5] S.C. Li, B. Varatharajan, F.A. Williams, Chemistry of JP-10 ignition, AIAA J. 39 (12) (2001) 2351–2356, doi:10.2514/2.1241.
- [6] C.K. Westbrook, W.J. Pitz, O. Herbinet, H.J. Curran, E.J. Silke, A comprehensive detailed chemical kinetic reaction mechanism for combustion of n-alkane hydrocarbons from n-octane to n-hexadecane, Combust. Flame 156 (1) (2009) 181-199. doi:10.1016/i.combustflame.2008.07.014.
- [7] H. Wang, R. Xu, K. Wang, C.T. Bowman, R.K. Hanson, D.F. Davidson, K. Brezinsky, F.N. Egolfopoulos, A physics-based approach to modeling real-fuel combustion chemistry I. Evidence from experiments, and thermodynamic, chemical kinetic and statistical considerations, Combust. Flame 193 (2018) 502–519, doi:10.1016/J.COMBUSTFLAME.2018.03.019.
- [8] Y. Tao, G.P. Smith, H. Wang, Critical kinetic uncertainties in modeling hydrogen / carbon monoxide, methane, methanol, formaldehyde, and ethylene combustion, Combust. Flame 195 (2018) 18–29, doi:10.1016/j.combustflame.2018. 02.006.
- [9] R. Xu, K. Wang, S. Banerjee, J. Shao, T. Parise, Y. Zhu, S. Wang, A. Movaghar, D.J. Lee, R. Zhao, X. Han, Y. Gao, T. Lu, K. Brezinsky, F.N. Egolfopoulos,

- D.F. Davidson, R.K. Hanson, C.T. Bowman, H. Wang, A physics-based approach to modeling real-fuel combustion chemistryll. Reaction kinetic models of jet and rocket fuels, Combust. Flame 193 (2018) 520–537, doi:10.1016/J. COMBUSTFLAME.2018.03.021.
- [10] W.K. Metcalfe, S.M. Burke, S.S. Ahmed, H.J. Curran, A hierarchical and comparative kinetic modeling study of C1-C2 hydrocarbon and oxygenated fuels, Int. J. Chem. Kinet. 45 (10) (2013) 638–675, doi:10.1002/kin.20802.
- [11] W. Liu, A.P. Kelley, C.K. Law, Flame propagation and counterflow nonpremixed ignition of mixtures of methane and ethylene, Combust. Flame 157 (5) (2010) 1027–1036, doi:10.1016/j.combustflame.2009.11.002.
- [12] W. Lowry, J. De Vries, M. Krejci, E. Petersen, Z. Serinyel, W. Metcalfe, H. Curran, G. Bourque, Laminar flame speed measurements and modeling of pure alkanes and alkane blends at elevated pressures, J. Eng. Gas Turb. Power 133 (9) (2011) 1–9, doi:10.1115/1.4002809.
- [13] S. Ravi, T.G. Sikes, A. Morones, C.L. Keesee, E.L. Petersen, Comparative study on the laminar flame speed enhancement of methane with ethane and ethylene addition, Proc. Combust. Inst. 35 (1) (2015) 679–686, doi:10.1016/j.proci.2014. 05.120
- [14] C.K. Westbrook, An analytical study of the shock tube ignition of mixtures of methane and ethane, Combust. Sci. Technol. 20 (1–2) (1979) 5–17, doi:10.1080/ 00102207908946891.
- [15] E.L. Petersen, J.M. Hall, S.D. Smith, J. de Vries, A.R. Amadio, M.W. Crofton, Ignition of lean methane-based fuel blends at gas turbine pressures, J. Eng. Gas Turb. Power 129 (4) (2007) 937–944, doi:10.1115/1.2720543.
- [16] M.M. Holton, P. Gokulakrishnan, M.S. Klassen, R.J. Roby, G.S. Jackson, Autoignition delay time measurements of methane, ethane, and propane pure fuels and methane-based fuel blends, J. Eng. Gas Turb. Power 132 (9) (2010) 1–9, doi:10.1115/1.4000590.
- [17] C.J. Aul, W.K. Metcalfe, S.M. Burke, H.J. Curran, E.L. Petersen, Ignition and kinetic modeling of methane and ethane fuel blends with oxygen: a design of experiments approach, Combust. Flame 160 (7) (2013) 1153–1167, doi:10.1016/j.combustflame.2013.01.019.
- [18] J. Shao, D.F. Davidson, R.K. Hanson, A shock tube study of ignition delay times in diluted methane, ethylene, propene and their blends at elevated pressures, Fuel 225 (March) (2018) 370–380, doi:10.1016/j.fuel.2018.03.146.
- [19] M. Baigmohammadi, V. Patel, S. Nagaraja, A. Ramalingam, S. Martinez, S. Panigrahy, A.A.E.S. Mohamed, K.P. Somers, U. Burke, K.A. Heufer, A. Pekalski, H.J. Curran, Comprehensive experimental and simulation study of the ignition delay time characteristics of binary blended methane, ethane, and ethylene over a wide range of temperature, pressure, equivalence ratio, and dilution, Energy Fuels 34 (7) (2020) 8808–8823, doi:10.1021/acs.energyfuels.0c00960.
- [20] A.V. Joshi, H. Wang, Master equation modeling of wide range temperature and pressure dependence of CO + OH products, Int. J. Chem. Kinet. 38 (1) (2006) 57–73, doi:10.1002/kin.20137.
- [21] R. Hanson, D. Davidson, Recent advances in laser absorption and shock tube methods for studies of combustion chemistry, Prog. Energy Combust. Sci. 44 (2014) 103–114, doi:10.1016/j.pecs.2014.05.001.
- [22] C.-L. Yu, C. Wang, M. Frenklach, Chemical kinetics of methyl oxidation by molecular oxygen, J. Phys. Chem. 99 (39) (1995) 14377–14387, doi:10.1021/ j100039a027.
- [23] W. Ren, A. Farooq, D.F. Davidson, R.K. Hanson, CO concentration and temperature sensor for combustion gases using quantum-cascade laser absorption near 4.7 μm, Appl. Phys. B 107 (3) (2012) 849–860, doi:10.1007/s00340-012-5046-1.
- [24] S.H. Pyun, W. Ren, K.Y. Lam, D.F. Davidson, R.K. Hanson, Shock tube measurements of methane, ethylene and carbon monoxide time-histories in DME pyrolysis, Combust. Flame 160 (4) (2013) 747–754, doi:10.1016/j.combustflame. 2012.12.004.
- [25] W. Ren, R.M. Spearrin, D.F. Davidson, R.K. Hanson, Experimental and modeling study of the thermal decomposition of C3–C5 ethyl esters behind reflected shock waves, J. Phys. Chem. A 118 (10) (2014) 1785–1798, doi:10.1021/jp411766b.
- [26] F. Sen, B. Shu, T. Kasper, J. Herzler, O. Welz, M. Fikri, B. Atakan, C. Schulz, Shock-tube and plug-flow reactor study of the oxidation of fuel-rich CH₄/O₂ mixtures enhanced with additives, Combust. Flame 169 (2016) 307–320, doi:10.1016/j.combustflame.2016.03.030.
- [27] C.R. Mulvihill, S.A. Alturaifi, E.L. Petersen, High-temperature He- and O₂-broadening of the R(12) line in the 1←0 band of carbon monoxide, J. Quant. Spectrosc. Radiat.Transf. 217 (2018) 432–439, doi:10.1016/j.jqsrt.2018.06.015.
- [28] C.R. Mulvihill, C.L. Keesee, T. Sikes, R.S. Teixeira, O. Mathieu, E.L. Petersen, Ignition delay times, laminar flame speeds, and species time-histories in the H₂S/CH₄ system at atmospheric pressure, Proc. Combust. Inst. 37 (1) (2019) 735–742, doi:10.1016/j.proci.2018.06.034.
- [29] O. Mathieu, C.R. Mulvihill, E.L. Petersen, Assessment of modern detailed kinetics mechanisms to predict CO formation from methane combustion using shock-tube laser-absorption measurements, Fuel 236 (2019) 1164–1180, doi:10.1016/j.fuel.2018.09.029.
- [30] D. He, D. Nativel, J. Herzler, J.B. Jeffries, M. Fikri, C. Schulz, Laser-based CO concentration and temperature measurements in high-pressure shock-tube studies of n-heptane partial oxidation, Appl. Phys. B 126 (8) (2020) 1–11, doi:10.1007/s00340-020-07492-7.
- [31] D. He, L. Shi, D. Nativel, J. Herzler, M. Fikri, C. Schulz, CO-concentration and temperature measurements in reacting CH₄/O₂ mixtures doped with diethyl ether behind reflected shock waves, Combust. Flame 216 (2020) 194–205, doi:10.1016/j.combustflame.2020.02.024.

- [32] C.F. Goldsmith, L.B. Harding, Y. Georgievskii, J.A. Miller, S.J. Klippenstein, Temperature and pressure-dependent rate coefficients for the reaction of vinyl radical with molecular oxygen, J. Phys. Chem. A 119 (28) (2015) 7766–7779, doi:10.1021/acs.ipca.5b01088.
- [33] N.J. Labbe, R. Sivaramakrishnan, C.F. Goldsmith, Y. Georgievskii, J.A. Miller, S.J. Klippenstein, Weakly bound free radicals in combustion: prompt dissociation of formyl radicals and its effect on laminar flame speeds, J. Phys. Chem. Lett. 7 (1) (2016) 85–89, doi:10.1021/acs.jpclett.5b02418.
- [34] N.J. Labbe, R. Sivaramakrishnan, C.F. Goldsmith, Y. Georgievskii, J.A. Miller, S.J. Klippenstein, Ramifications of including non-equilibrium effects for HCO in flame chemistry, Proc. Combust. Inst. 36 (1) (2017) 525–532, doi:10.1016/j. proci.2016.06.038.
- [35] D.I. Pineda, F.A. Bendana, K.K. Schwarm, R.M. Spearrin, Multi-isotopologue laser absorption spectroscopy of carbon monoxide for high-temperature chemical kinetic studies of fuel mixtures, Combust. Flame 207 (2019) 379–390, doi:10.1016/j.combustflame.2019.05.030.
- [36] A. Eveleigh, N. Ladommatos, Isotopic tracers for combustion research, Combust. Sci. Technol. 189 (4) (2017) 660–682, doi:10.1080/00102202.2016. 1246440.
- [37] I. Stranic, G.A. Pang, R.K. Hanson, D.M. Golden, C.T. Bowman, Shock tube measurements of the tert -Butanol + OH Reaction Rate and the tert - C_4H_8 OH Radical β -Scission Branching Ratio Using Isotopic Labeling, TheJournal of Physical Chemistry A 117 (23) (2013) 4777–4784, doi:10.1021/jp402176e.
- [38] G.P. Smith, D.M. Golden, M. Frenklach, N.W. Moriarty, B. Eiteneer, M. Goldenberg, C.T. Bowman, R.K. Hanson, S. Song, W.C. Gardiner, V.V. Lissianski, Z. Qin, GRI-MECH 3.0, 1999, (http://www.me.berkeley.edu/gri_mech/). Version 3.0.
- [39] R.K. Hanson, R.M. Spearrin, C.S. Goldenstein, Spectroscopy and Optical Diagnostics for Gases, Springer International Publishing, Cham, 2016, doi:10.1007/ 978-3-319-23252-2.
- [40] A.P. Nair, D.D. Lee, D.I. Pineda, J. Kriesel, W.A. Hargus, J.W. Bennewitz, S.A. Danczyk, R.M. Spearrin, MHz laser absorption spectroscopy via diplexed RF modulation for pressure, temperature, and species in rotating detonation rocket flows, Appl. Phys. B 126 (8) (2020) 138, doi:10.1007/s00340-020-07483-8
- [41] M. Röhrig, E.L. Petersen, D.F. Davidson, R.K. Hanson, A shock tube study of the pyrolysis of NO₂, Int. J. Chem. Kinet. 29 (7) (1997) 483–493, doi:10.1002/(SICI) 1097-4601(1997)29:7<483::AID-KIN2>3.0.CO;2-Q.
- [42] M.F. Campbell, K.G. Owen, D.F. Davidson, R.K. Hanson, Dependence of calculated postshock thermodynamic variables on vibrational equilibrium and input uncertainty, J. Thermophys. Heat Transf. 31 (3) (2017) 586–608, doi:10.2514/1. T4952
- [43] E.L. Petersen, R.K. Hanson, Nonideal effects behind reflected shock waves in a high-pressure shock tube, Shock Waves 10 (6) (2001) 405-420, doi:10.1007/ PI.00004051.

- [44] M.F. Campbell, T. Parise, A.M. Tulgestke, R.M. Spearrin, D.F. Davidson, R.K. Hanson, Strategies for obtaining long constant-pressure test times in shock tubes, Shock Waves 25 (6) (2015) 651–665, doi:10.1007/s00193-015-0596-x.
- [45] F.A. Bendana, D.D. Lee, C. Wei, D.I. Pineda, R.M. Spearrin, Line mixing and broadening in the ν(1→3) first overtone bandhead of carbon monoxide at high temperatures and high pressures, J. Quant. Spectrosc. Radiat.Transf. 239 (2019) 106636, doi:10.1016/j.jqsrt.2019.106636.
- [46] D.D. Lee, F.A. Bendana, A.P. Nair, D.I. Pineda, R.M. Spearrin, Line mixing and broadening of carbon dioxide by argon in the v_3 bandhead near 4.2 μ m at high temperatures and high pressures, J. Quant. Spectrosc. Radiat.Transf. 253 (2020) 107135, doi:10.1016/j.jqsrt.2020.107135.
- [47] M.A. Oehlschlaeger, D.F. Davidson, J.B. Jeffries, Temperature measurement using ultraviolet laser absorption of carbon dioxide behind shock waves, Appl. Opt. 44 (31) (2005) 6599, doi:10.1364/AO.44.006599.
- [48] Z. Hong, G.A. Pang, S.S. Vasu, D.F. Davidson, R.K. Hanson, The use of driver inserts to reduce non-ideal pressure variations behind reflected shock waves, Shock Waves 19 (2) (2009) 113–123, doi:10.1007/s00193-009-0205-y.
- [49] G.P. Smith, Y. Tao, H. Wang, Foundational fuel chemistry model version 1.0 (FFCM-1), 2016, (http://nanoenergy.stanford.edu/FFCM-1). Version 1.0.
- [50] D.G. Goodwin, R.L. Speth, H.K. Moffat, B.W. Weber, Cantera: an object-oriented software toolkit for chemical kinetics, thermodynamics, and transport processes, 2018, (https://www.cantera.org). Version 2.4.0. 10.5281/zenodo.1174508
 [51] H. Li, Z.C. Owens, D.F. Davidson, R.K. Hanson, A simple reactive gasdynamic
- [51] H. Li, Z.C. Owens, D.F. Davidson, R.K. Hanson, A simple reactive gasdynamic model for the computation of gas temperature and species concentrations behind reflected shock waves, Int. J. Chem. Kinet. 40 (4) (2008) 189–198, doi:10.1002/kin.20305.
- [52] H. Wang, X. You, A.V. Joshi, S.G. Davis, A. Laskin, F. Egolfopoulos, C.K. Law, USC Mech version II. High-temperature combustion reaction model of H₂/CO/C₁-C₄ compounds, 2007, (http://ignis.usc.edu/USC_Mech_II.htm).
- [53] C.W. Zhou, Y. Li, E. O'Connor, K.P. Somers, S. Thion, C. Keesee, O. Mathieu, E.L. Petersen, T.A. DeVerter, M.A. Oehlschlaeger, G. Kukkadapu, C.J. Sung, M. Alrefae, F. Khaled, A. Farooq, P. Dirrenberger, P.A. Glaude, F. Battin-Leclerc, J. Santner, Y. Ju, T. Held, F.M. Haas, F.L. Dryer, H.J. Curran, A comprehensive experimental and modeling study of isobutene oxidation, Combust. Flame 167 (2016) 353–379, doi:10.1016/j.combustflame.2016.01.021.
- [54] K. Narayanaswamy, G. Blanquart, H. Pitsch, A consistent chemical mechanism for oxidation of substituted aromatic species, Combust. Flame 157 (10) (2010) 1879–1898, doi:10.1016/j.combustflame.2010.07.009.
- [55] D.F. Davidson, Y. Zhu, J. Shao, R.K. Hanson, Ignition delay time correlations for distillate fuels, Fuel 187 (2017) 26–32, doi:10.1016/j.fuel.2016.09.047.